2014 IEEE International Conference on Robotics & Automation (ICRA)
Hong Kong Convention and Exhibition Center
May 31 - June 7, 2014. Hong Kong, China

Experimental Evaluation of Adaptive Model-Based Control for Underwater Vehicles In the Presence of Unmodeled Actuator Dynamics

Christopher J. McFarland and Louis L. Whitcomb

***Abstract*— This paper reports a comparative experimental evaluation of proportional derivative and adaptive model-based control for underwater vehicles. To the best of the authors' knowledge, this is the first such evaluation of model-based adaptive tracking control for underwater vehicles during simultaneous dynamic motion in all 6 degrees-of-freedom. This experimental evaluation revealed the presence of unmodeled thruster dynamics arising during reversals of the vehicle's thrusters, and that the unmodeled thruster dynamics can destabilize parameter adaptation. The three major contributions of this paper are: an experimental analysis of how unmodeled thruster dynamics can destabilize parameter adaptation, a two-step adaptive model-based control algorithm which is robust to the thruster modeling errors present, and a comparative experimental evaluation of adaptive model-based control and proportional derivative control for fully-actuated underwater vehicles preforming simultaneous 6 degree-of-freedom trajectory tracking.**

I. INTRODUCTION

This paper addresses the problem of adaptive model-based trajectory tracking control of Underwater Vehicles (UV) for dynamic 6 degree-of-freedom (DOF) motion. The approach of adaptive model-based control (AMBC) refines estimates of plant parameters during the trajectory tracking control process. The adaptive controller estimates parameters for a rigid-body plant such as vehicle mass with added hydrodynamic mass, quadratic drag, gravitational force, and buoyancy torque parameters that arise in the dynamic models of rigid-body UV. We report a comparative experimental evaluation of AMBC and proportional derivative control (PDC) in full scale vehicle trials utilizing the Johns Hopkins University Hydrodynamic Test Facility and Johns Hopkins University Remotely Operated Vehicle (JHU ROV) (Fig. 1). This experimental evaluation shows that AMBC provides 30% better position tracking performance and 8% worse velocity tracking performance over PDC. To the best of the authors' knowledge, this is the first experimental comparison of AMBC and PDC during simultaneous motion in all DOF.

This paper is organized as follows: Section II states two UV control algorithms: a non-adaptive model-based controller (MBC) which assumes knowledge of the plant parameters and an adaptive model-based controller which estimates plant parameters during the control process. Both approaches can be shown to provide asymptotically exact trajectory tracking in position and velocity [16]. Section II-C reports a two-step AMBC algorithm which is shown experimentally to be robust to the actuator modeling errors observed in our experimental vehicle. Section III-C presents two experiments where AMBC is used to follow a pitch only reference trajectory. The range of motion is changed such that one pitch only reference trajectory requires thrust reversals and the other pitch only reference trajectory does not. A comparative analysis of these parameter adaption processes details how unmodeled dynamics arising from thrust reversals can cause unstable parameter adaptation. Section III-C also shows how direct implementation of the AMBC from Theorem 2.1 exhibits unstable parameter adaptation in the presence of unmodeled thrust reversal dynamics. Section III-D reports an experimental evaluation of the two-step AMBC algorithm, and a comparison of AMBC and PDC.

This work was supported by the National Science Foundation under Award 0812138 and 1319667. Support for the first author was provided by the Link Foundation and ARCS Foundation.

The authors are with the Department of Mechanical Engineering, Johns Hopkins University, Baltimore, MD 21218, USA, cmcfarland, llw@jhu.edu

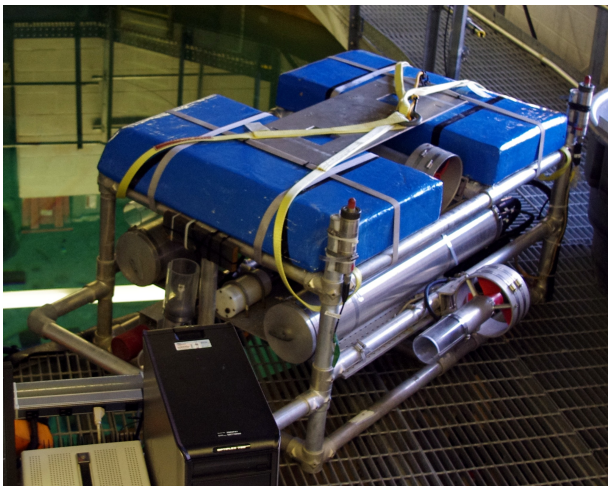

Fig. 1: JHU ROV inside the Johns Hopkins Hydrodynamic Test Facility.

A. Background and Paper Contribution

Recent advances in UV enabling technologies including *in-situ* sensing, power storage, and communication modalities have enabled the development of UVs which can accomplish missions previously thought impractical or impossible. Many of these missions, such as commercial seafloor surveys and environmental monitoring, depend on tracking a specified trajectory as closely as possible. To facilitate these missions, novel UV control algorithms are required to provide improved trajectory tracking precision. UV MBC has been shown experimentally to provide significant performance gains over PDC [15], however MBC requires model parameters to be known *a priori*. UV AMBC removes the need for a previously identified model. Although a few experimental implementations UV AMBC algorithms have

been reported, experimental evaluations of AMBC during simultaneous motion in all DOF is a lacuna in the literature.

In *steady-state* operation at zero advance velocity the axial thrust of a bladed-propeller marine thruster is linearly proportional to the applied shaft torque, and is also linearly proportional to the signed-square of the shaft angular velocity [26]. The parameters of these steady-state thruster models cannot be determined analytically, but are easily estimated with simple steady-state experiments. Research by the author and others has shown that the *transient* performance of marine thrusters can be accurately approximated by a finite-dimensional second-order plant model of propeller-fluid interaction [2], [8], [10], [28]. The plant parameters of these dynamic thruster models cannot be determined analytically, and are very difficult to measure experimentally because such identification requires highly instrumented measurements of both the thruster and the fluid in unsteady operation.

Because unsteady thruster model parameters are difficult to obtain experimentally, in the design of marine vehicle control systems it is common practice to employ easily-obtained steady-state thruster models. This approach works extremely well for steady-state or slowly time-varying vehicles motion, but results in the presence of unmodeled thruster dynamics during highly dynamic vehicle maneuvering. In 1984 Rohrs et al. famously showed that stable adaptive controllers for linear time-invariant plants can be destabilized by the presence of unmodeled plant dynamics [21]. To the best of our knowledge, this paper reports the first observation of unmodeled thruster dynamics resulting in the destabilization of model-based adaptive tracking control of a UV.

B. Literature Review

Adaptive controllers for linear plants are well understood [18]. Adaptive reference trajectory-tracking is well understood for several types of second-order holonomic nonlinear plants whose parameters enter linearly into the plant equations of motion, e.g. robot manipulator arms [5], [22], [24], spacecraft [12], [23], and rigid-body rotational plants [4]. Comparative experimental evaluations of AMBC for robot manipulator arms have been performed, e.g. [19], [27].

[3] reports a PDC control law for a second-order rigid-body plant in free space using exponential error coordinates. UV MBC algorithms have been reported [7], with several experimental studies for control of the x, y, depth, and heading DOF [25], and for simultaneous motion in all DOF [15]. Previous studies have utilized a nonlinear model (such as (1)) in the development of tracking control algorithms which are robust to model parameter uncertainty. In [30] a sliding mode controller and numerical simulations of performance in X, Y and heading is reported. In [31] a discrete time parameter adaptation algorithm is reported with a numerical simulation study. In [6] the authors report a hybrid (adaptive and sliding) nonlinear UV controller which explicitly handles multiplicative uncertainty in the input mapping. The first experimental evaluation of nonlinear adaptive sliding-mode control on an underwater vehicle was reported [29]. In [32] an experimental evaluation of UV AMBC performance in the presence of noisy position readings is reported. In [1] an experimental evaluation of an AMBC is reported during simultaneous motion in the translational DOF. Comparative experimental evaluations of linear controllers, model-based controllers and their adaptive extensions for UV single DOF motion have been reported [13], [25]. In [33] a comparative experimental evaluation in the presence of a common external disturbance for proportional integral derivative control, disturbance observer control and the adaptive extensions of both is reported. In each of these experimental evaluations at most two DOF had a non-zero reference velocity at a given moment, and in all cases only set-point regulation was reported in the pitch and roll DOF.

C. Problem Statement

Notation: We represent the actual pose of the vehicle in exponential coordinates as $\psi_a \in \mathbb{R}^6$ and the actual velocity of the vehicle as ${}^a v_a \in \mathbb{R}^6$. Note that for ${}^w_a R \in \mathrm{SO}(3)$, the rotation matrix from the actual body-frame to the world-frame, and $p_a \in \mathbb{R}^3$, the position of the vehicle, we have ${}^w_a H = \begin{bmatrix} {}^w_a R & p_a \\ 0_{1\times 3} & 1 \end{bmatrix} = e^{\widehat{\psi_a}}$ where $\widehat{\ }: \mathbb{R}^6 \to \mathrm{se}(3)$ is the standard operator mapping $\mathbb{R}^6$ into the tangent space of $\mathrm{SE}(3)$ [17]. The vehicle's velocity vector obeys the relation ${}^a v_a = \begin{bmatrix} {}^a\nu_a^T & {}^a\omega_a^T \end{bmatrix}^T$, where ${}^a\nu_a \in \mathbb{R}^3$ is the vehicle's body-frame translational velocity and ${}^a\omega_a \in \mathbb{R}^3$ is the vehicle's body-frame angular velocity. We similarly represent the desired pose and velocity of the vehicle as $\psi_d \in \mathbb{R}^6$ and ${}^d v_d \in \mathbb{R}^6$ with the desired-frame homogeneous matrix, rotation matrix, position, translational velocity and angular velocity represented as ${}^w_d H$, ${}^w_d R$, p_d, ${}^d\nu_d$, and ${}^d\omega_d$, respectively.

Vehicle Dynamics: We model a UV as a rigid body with added hydrodynamic mass, quadratic drag, gravitational force, and buoyancy moving under the influence of external control torques $\tau \in \mathbb{R}^3$ and control forces $f \in \mathbb{R}^3$ applied by the vehicles thrusters. The commonly accepted second-order finite-dimensional lumped parameter dynamic model for a fully submerged rigid-body UV, in the body frame, is

$$\begin{aligned} {}^w_a \dot{H} &= {}^w_a H \widehat{{}^a v_a} \\ M {}^a\dot{v}_a &= \mathrm{ad}^T_{{}^a v_a} M {}^a v_a + \mathcal{D}({}^a v_a) + \mathcal{G}({}^w_a H) + u \end{aligned} \qquad (1)$$

where $\mathcal{D}(v) = \sum_{i=1}^6 |v_i| D_i v$, $\mathcal{G}(R) = \begin{bmatrix} gR^T e_3 \\ \mathcal{J}(b) R^T e_3 \end{bmatrix}$, $e_3 = [0\ 0\ 1]^T$, $u = \begin{bmatrix} f^T & \tau^T \end{bmatrix}^T$, $M \in \mathbb{R}^{6\times 6}$ is the vehicle's symmetric positive definite (SPD) mass matrix, the set $D_i \in \mathbb{R}^{6\times 6}$ $(i = 1 \cdots 6)$ are the 6 DOF fully-coupled quadratic drag coefficients, $g \in \mathbb{R}$ is the net vertical force acting on the vehicle due to gravity and buoyancy (i.e. the net buoyancy), and $b \in \mathbb{R}^3$ is the moment applied to the vehicle due to the relative positions of the center-of-gravity and center-of-buoyancy (which will vary as a function of the vehicle's roll and pitch) [7]. We assume ${}^w_a H$, ${}^a v_a$, f and τ are accessible signals and the parameters (M, $D_{i,i=1\cdots 6}$, g, b) are constant but unknown. Note that (1) is linear in M, D, g and b, thus can be parametrized as a single parameter vector, $\theta \in \mathbb{R}^{241}$ with M having 21 parameters, D having 216 parameters, g having 1 parameter, and b having 3 parameters.

The functions $\mathcal{J}: \mathbb{R}^3 \to \mathbb{R}^{3\times 3}$ (the mapping from $\mathbb{R}^3$ to so(3)), $\widehat{\ }: \mathbb{R}^6 \to \mathbb{R}^{4\times 4}$ (the mapping from $\mathbb{R}^6$ to se(3)), ad :

$\mathbb{R}^6 \to \mathbb{R}^{6\times 6}$ (the se(3) adjoint operator), and $\mathrm{Ad} : \mathrm{SE}(3) \to \mathbb{R}^{6\times 6}$ (the se(3) adjoint map) and further information on state representation, the parameters analytic properties, the structure of θ, state error representations, the SE(3) logorithm $\log_{\mathrm{SE}(3)} : \mathrm{SE}(3) \to \mathrm{se}(3)$ and the inverse SE(3) Velocity Jacobian $\hat{\mathcal{A}}^{-1} : \mathrm{se}(3) \to \mathbb{R}^{6\times 6}$ are detailed in [16].

Error Coordinates: We define ΔH as

$$\Delta H = {}^{w}_{d}H^{-1}\,{}^{w}_{a}H. \tag{2}$$

We use ΔH to define the position tracking error ($\Delta\psi$), velocity tracking error (Δv), and parameter error vector as

$$\Delta\psi = \log_{\mathrm{SE}(3)}(\Delta H) \tag{3}$$

$$\Delta v = {}^{a}v_a - {}^{a}v_d \tag{4}$$

$$\Delta\theta = \hat{\theta} - \theta \tag{5}$$

where ${}^{a}v_d = \mathrm{Ad}_{\Delta H^{-1}}\,{}^{d}v_d$.

Norm and Eigenvalue Conventions: We employ the following notation convention for the eigenvalues of the mass matrix: $\hat{\lambda}_6$ is the smallest and $\hat{\lambda}_1$ is the largest eigenvalues of the mass matrix $\hat{M}(t)$, the other eigenvalues are labeled such that $\hat{\lambda}_{i-1}(t) \leq \hat{\lambda}_i(t) \leq \hat{\lambda}_{i+1}(t)$. The eigenvalues of M and ΔM are labeled using the same convention.

Goal: Given a desired trajectory $\{{}^{w}_{d}H, {}^{d}v_d, {}^{d}\dot{v}_d\}$ for a plant of the form (1) with unknown plant parameters $\{M, D, g, b\}$, our goal is to develop a control law $u : \mathrm{SE}(3)\times\mathbb{R}^6 \times \mathrm{SE}(3)\times\mathbb{R}^6 \times \mathbb{R}^6 \times \mathbb{R}^{241} \to \mathbb{R}^6$ and parameter update law $\dot{\hat{\theta}} : \mathrm{SE}(3)\times\mathbb{R}^6 \times \mathrm{SE}(3)\times\mathbb{R}^6 \times \mathbb{R}^6 \to \mathbb{R}^{241}$ which guarantee that all signals remain bounded and provide asymptotically exact reference tracking, i.e. $\lim_{t\to\infty}\Delta\psi(t) = \vec{0}$ and $\lim_{t\to\infty}\Delta v(t) = \vec{0}$.

II. UV Adaptive Model-Based Tracking Control

This Section states three tracking control algorithms for mechanical plants of the form (1): a MBC, an AMBC, and a two-step AMBC. All three tracking controllers reported herein admit the use of a fully-coupled model for UV dynamics; however, to clarify the analysis of UV AMBC in the presence of unmodeled thruster dynamics, we implemented controllers which employ an uncoupled model of UV dynamics for the experimental evaluations reported in Section III. Note that the MBC requires exact *a priori* parameter knowledge, whereas the AMBC provides asymptotically exact tracking control without requiring *a priori* knowledge of the plant parameters.

A. UV Model-Based Tracking Controller

Theorem 1.1: For plants of the form (1), when the plant parameters, θ, are known, the control law

$$\begin{aligned} &u\left({}^{w}_{a}H, {}^{a}v_a, {}^{w}_{d}H, {}^{d}v_d, {}^{d}\dot{v}\right) \\ &= -\left(k_p\hat{\mathcal{A}}^{-T}(\Delta\psi) + k_d\Delta v\right) + \mathbb{W}({}^{a}\dot{v}_d, \Delta v, {}^{a}v_d, {}^{w}_{a}H)\theta, \end{aligned} \tag{6}$$

where the regressor matrix $\mathbb{W} : \mathbb{R}^6 \times \mathbb{R}^6 \times \mathbb{R}^6 \times \mathrm{SE}(3) \to \mathbb{R}^{6\times 241}$ is defined such that

$$\begin{aligned} \mathbb{W}({}^{a}\dot{v}_d, \Delta v, {}^{a}v_d, {}^{w}_{a}H)\theta =& M{}^{a}\dot{v}_d - M\,\mathrm{ad}_{\Delta v}\,{}^{a}v_d - \mathrm{ad}^{T}_{{}^{a}v_a}M{}^{a}v_a \\ &- \mathcal{D}({}^{a}v_a) - \mathcal{G}({}^{w}_{a}H), \end{aligned} \tag{7}$$

provides asymptotically stable trajectory tracking in the sense of Lyapunov, i.e. $\lim_{t\to\infty}\Delta\psi(t) = \vec{0}$ and $\lim_{t\to\infty}\Delta v(t) = \vec{0}$, if the following conditions are met:

- the signals $\{{}^{w}_{d}H, {}^{d}v_d, {}^{d}\dot{v}_d\} \in \{\mathrm{SE}(3), \mathbb{R}^6, \mathbb{R}^6\}$ are continuous and bounded
- $k_d.k_p \in \mathbb{R}_+$
- $\|x(t_0)\| < \sqrt{\frac{\epsilon\lambda_{12}}{{}_{\epsilon}\lambda_1}}\pi$

where, as per the eigenvalue ordering conventions from Section I-C, ${}_{\epsilon}\lambda_i$ are the eigenvalues of

$$\mathcal{M}_\epsilon = \begin{bmatrix} k_p\mathbb{I}_{6\times 6} & \epsilon M \\ \epsilon M & M \end{bmatrix}. \tag{8}$$

A stability proof is reported in [16].

B. UV Adaptive Model-Based Tracking Controller

Theorem 2.1: For plants of the form (1) with unknown plant parameters θ the control and parameter update laws

$$\begin{aligned} &u({}^{w}_{a}H, {}^{a}v_a, {}^{w}_{d}H, {}^{d}v_d, {}^{d}\dot{v}, \hat{\theta}) \\ &= -\left(k_p\hat{\mathcal{A}}^{-T}(\Delta\psi) + k_d\Delta v\right) + \mathbb{W}({}^{a}\dot{v}_d, \Delta v, {}^{a}v_d, {}^{w}_{a}H)\hat{\theta} \end{aligned} \tag{9}$$

$$\begin{aligned} &\dot{\hat{\theta}}({}^{w}_{a}H, {}^{a}v_a, {}^{w}_{d}H, {}^{d}v_d, {}^{d}\dot{v}_d) \\ &= -K_\theta\mathbb{W}^T({}^{a}\dot{v}_d, \Delta v, {}^{a}v_d, {}^{w}_{a}H)(\epsilon\Delta\psi + \Delta v) \end{aligned} \tag{10}$$

provide asymptotically stable trajectory tracking in the sense of Lyapunov, i.e. $\lim_{t\to\infty}\Delta\psi(t) = \vec{0}$ and $\lim_{t\to\infty}\Delta v(t) = \vec{0}$, and the parameter values converge to constant values, i.e. $\lim_{t\to\infty}\dot{\hat{\theta}}(t) = 0_{241\times 1}$, if the following conditions are met:

- the signals $\{{}^{w}_{d}H, {}^{d}v_d, {}^{d}\dot{v}_d\} \in \{\mathrm{SE}(3), \mathbb{R}^6, \mathbb{R}^6\}$ are continuous and bounded
- $k_d, k_p \in \mathbb{R}_+$
- K_θ is SPD
- $\epsilon < \min\left(\frac{4k_pk_d}{2\lambda_1k_pc+k_d^2}, \sqrt{\frac{k_p\lambda_6}{\lambda_1^2}}\right)$
- $\sqrt{\frac{\epsilon\lambda_1}{{}_{\epsilon}\lambda_{12}}\|x(t_0)\|^2 + \frac{k_\theta}{{}_{\epsilon}\lambda_{12}}\|\Delta\theta(t_0)\|^2} < \pi$.

where $k_\theta = \frac{1}{\min\mathrm{eig}\,K_\theta}$, ${}_{\epsilon}\lambda_i$ are the eigenvalues of $\mathcal{M}_\epsilon$, and λ_i are the eigenvalues of M (noting the eigenvalue conventions from Section I-C). A stability proof is reported in [16].

C. Two-Step AMBC

(1) allows the identification of dynamic and gravitational parameters to be conducted in a two-step process. (7) is linear in the parameters, thus there exists a set of regressor vectors $\mathbb{W}_i : \mathbb{R}^6 \times \mathbb{R}^6 \times \mathbb{R}^6 \times \mathrm{SE}(3) \to \mathbb{R}^6$ such that

$$\sum_{i=1}^{241}\mathbb{W}_i({}^{a}\dot{v}_d, \Delta v, {}^{a}v_d, {}^{w}_{a}H)\theta_i = \mathbb{W}({}^{a}\dot{v}_d, \Delta v, {}^{a}v_d, {}^{w}_{a}H)\theta. \tag{11}$$

If a subset of parameter values in θ is known *a priori* then, based on Theorems 1.1 and 2.1, an AMBC can be developed to estimate the remaining unknown parameters. Any AMBC of this form achieve asymptotically exact trajectory tracking canceling the contribution to vehicle dynamics due to known parameters (Section 1.1) and use parameter update laws to adaptively learn estimates of the unknown parameters (Section 2.1). If K_θ is assumed to be diagonal, each AMBC of this form will be equivalent to using the AMBC from Theorem 2.1 with each known parameter initialized to its known value and its associated parameter gain within K_θ set to zero. The two-step AMBC presented herein relies on independently estimating two disparate sets of parameters.

The first step is identifying the g and b during slow (quasi-static) pitch and roll motion, for which the plant model

$$0 = \mathcal{G}({}^{w}_{a}H) + u \tag{12}$$

is valid—where all inertial and drag terms are assumed to be negligible because they are either quadratic in velocity or linear in acceleration. The validity of this model implies using the adaptive tracking controller from Theorem 2.1 to track a slow reference trajectory in pitch and roll will identify estimates of g and b without requiring the simultaneous estimation of mass and drag parameters.

The second step AMBC estimates the inertial and drag parameters (i.e. M and D) while using the gravitational parameter values identified in step one. Using the controller from Theorem 2.1 with $\hat{b}(t_0)$ and $\hat{g}(t_0)$ set to their previously identified values, this controller can be used to track any reference trajectory while identifying estimates of the vehicle's mass and drag.

III. Experimental Evaluation

A. Experimental Setup

The JHU Hydrodynamic Test Facility [11] contains an indoor fresh water tank measuring $7.75\ \mathrm{m}$ in diameter and $4.25\ \mathrm{m}$ deep, as shown in Figure 1. The facility is equipped with the JHU ROV, a fully instrumented UV designed for navigation and control research. The JHU ROV displaces $150\ \mathrm{kg}$ and is actuated by six $1.5\ \mathrm{kWh}$ DC electric thrusters providing full control authority in 6 DOF. Each thruster is controlled with a current-mode amplifier in conjunction with data from *a-priori* thruster calibration experiments. We estimate thruster force (f_{th}) based on measured thruster angular velocities (ω_{th}) using the empirically validated steady state relation $f_{th} = k_{th}\omega_{th}|\omega_{th}|$ [26].

The world-frame's orthonormal x, y, and z unit vectors point from the frame's origin towards in the directions North, East and down respectively. Employing standard navel architecture convention, the body-frame's x, y, and z unit vectors point from the vehicle's origin toward, respectivly, the vehicle's bow, starboard side and keel [26].

The vehicle state is instrumented by a PHINS Inertial Navigation System (IXSEA SAS, Marly-le-Roi, France), $1200\ \mathrm{kHz}$ bottom-lock Doppler sonar (RD Instruments, San Diego, CA), and Paroscientfic depth sensor. The PHINS INS includes a three-axis north-seeking fiber-optic gyrocompass and inertial grade accelerometers whose data is used to estimate angular velocity, pitch, roll, and heading states at $10\ \mathrm{Hz}$. For our PHINS configuration, the measurement standard deviations are $0.01°$/s for angular velocity estimates, $0.13°$ for heading estimates, and $0.01°$ for pitch and roll estimates [9]. This Doppler sonar measures the three dimensional linear velocity in the instrument's frame to an accuracy of 0.3% with an update rate of $6\ \mathrm{Hz}$ and zero bias [20].

B. Experimental Testing Methodology

To evaluate the performance of the identified plant models we employ the approach that we term *cross-validation*. We use the plant model experimentally identified from a vehicle experimental identification trial to predict, in a numerical simulation, the performance of the actual plant in a different experimental trial whose trajectories differ from the experimental identification trial. The class of plants given by (1) are open-loop-stable in linear velocity and angular velocity due to the hydrodynamic damping. In the presence of significant buoyancy torque due to center-of-gravity to center-of-buoyancy separation, this class of plants is also open-loop-stable in roll and pitch. Because these open-loop signals are stable, we can employ these signals to compare the model plant's predicted performance to the actual plant's experimentally observed performance. The error between the predicted model performance and the experimentally observed performance is reported as the mean absolute error (MAE) between the simulated plant roll, pitch, linear velocity and angular velocity and the actual experimental plant roll, pitch, linear velocity and angular velocity. To compare the trajectory tracking performance of controllers we consider the mean normal of error (MNE) vectors, such as the position and velocity error vectors. Smaller NME magnitude means the plant is more closely tracking the reference trajectory.

The fully-coupled model of UV dynamics used in (1) requires 241 independent parameter values. To clarify the experimental analysis of UV AMBC in the presence of unmodeled thruster dynamics, we have implemented a controller which employs an uncoupled model using 16 scalar terms: 6 hydrodynamic mass, 6 quadratic drag terms (one for each DOF which we will label as m_i and d_i respectively), and the 4 gravitational parameters g and b. A recent comparative experimental study of the performance of several 6-degree of freedom (DOF) UV plant models (including both the uncoupled 16 plant parameter model and fully-coupled 241 plant parameter model) concluded that the fully coupled models (with 241 parameters) most accurately predict plant dynamic behavior for fully-coupled 6-DOF dynamic motion, however the 16 plant parameter model provided adequate predictive capacity [14]. For a diagonal parameter adaptation gain matrix K_θ, we can label the individual mass parameter gains as γ_{m_i}, the individual drag parameter gains as γ_{d_i}, the individual buoyancy parameter gains as γ_{b_i} and the gravitational parameter gain as γ_g. Sinusoidal reference trajectories are used in this study. Table I lists the frequencies and amplitudes for the 6 DOF reference trajectories used.

TABLE I: Reference Trajectory Information

		RefTraj1	RefTraj2
Reference Trajectory Propose		Parameter Identification	Parameter Cross-Validation
DOF	*Excitation*	*Trajectory-Tracking*	
world x	Cos Freq	0.242 rad/sec	0.185 rad/sec
	Cos Amp	0.50 m	0.50 m
DOF	*Excitation*	*Trajectory-Tracking*	
world y	Cos Freq	0.210 rad/sec	0.286 rad/sec
	Cos Amp	0.50 m	0.50 m
DOF	*Excitation*	*Trajectory-Tracking*	
world z	Cos Freq	0.185 rad/sec	0.242 rad/sec
	Cos Amp	0.30 m	0.30 m
DOF	*Excitation*	*Trajectory-Tracking*	*Torque Input*
roll	Cos Frequency	0.5 rad/sec	0.55 rad/sec
	Cos Amplitude	6.9°	35 N m
DOF	*Excitation*	*Trajectory-Tracking*	*Torque Input*
pitch	Cos Freq	0.6 rad/sec	0.65 rad/sec
	Cos Amp	8.6°	30 N m
DOF	*Excitation*	*Trajectory-Tracking*	
heading	Cos Freq	0.210 rad/sec	0.0824 rad/sec
	Cos Amp	135°	135°

C. Experimental Analysis of UV AMBC Instability

In this subsection we report the results from three experiments using AMBC to control the JHU ROV. Two experiments reveal parameter adaptation instability in the presence of unmodeled thruster dynamics during thrust reversals. A third experiment does not have thrust reversals and parameter estimates remain stable. In all three experiments the mass, drag, and gravitational terms were initialized to previously identified parameters values (Tables IV and V).

Tables II and III tabulate the initial and final parameters identified from the first experiment during simultaneous dynamic maneuvers in all DOF. For this experiment, the reference trajectory specified was RefTraj1 from Table I, and the gains used were $k_p = 300$, $k_d = 100$ $\gamma_{m_i} = 1000$, $\gamma_{d_i} = 5000$, $\gamma_g = \gamma_{b_1} = \gamma_{b_2} = 0.5$ and $\gamma_{b_3} = 10.0$. Over this two-hour duration experiment most parameter values oscillated near their previously identified values, however $\hat{b}_3(t)$, $\hat{m}_4(t)$, and $\hat{m}_5(t)$ adapted away from their previously identified values. As seen in Figure 2, these mass estimates adapt to physically unrealistic negative values and show no signs of asymptotic behavior.

TABLE II: Gravitational Parameters Identified During Unstable Parameter Adaptation

	g	b_1	b_2	b_3
Init	3.63 N	1.017 $N\,m$	3.02 $N\,m$	300 $N\,m$
Final	-5.71 N	2.6 $N\,m$	3.53 $N\,m$	261 $N\,m$

TABLE III: Mass and Drag Parameters Identified During Unstable Parameter Adaptation

DOF	$m_i(t_o)$	$m_i(t_f)$	$d_i(t_o)$	$d_i(t_f)$
Tran X	583 kg	583 kg	-1245 $\frac{N\,s^2}{m^2}$	-1005 $\frac{N\,s^2}{m^2}$
Tran Y	873 kg	769 kg	-1426 $\frac{N\,s^2}{m^2}$	-1400 $\frac{N\,s^2}{m^2}$
Tran Z	1021 kg	1031 kg	-3060 $\frac{N\,s^2}{m^2}$	-3039 $\frac{N\,s^2}{m^2}$
Ang X	103.5 $kg\,m^2$	-1.348 $kg\,m^2$	-728.4 $N\,s^2$	-761.5 $N\,s^2$
Ang Y	137.1 $kg\,m^2$	42.5 $kg\,m^2$	-769.1 $N\,s^2$	-681.4 $N\,s^2$
Ang Z	106.4 $kg\,m^2$	41 $kg\,m^2$	-376.2 $N\,s^2$	-393.3 $N\,s^2$

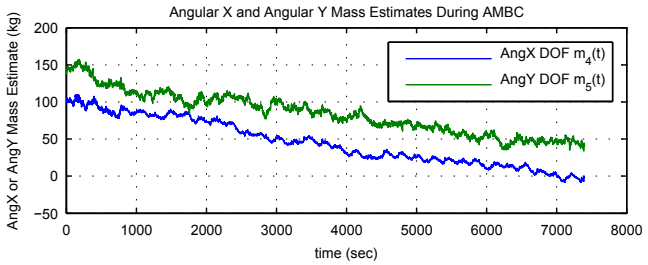

Fig. 2: The time evolution of of Angular X DOF and Angular Y DOF mass estimates from AMBC during 6 DOF dynamic maneuvers. These mass estimates adapt to physically unrealistic negative values and show no signs of asymptotic behavior.

The second and third experiments compare parameter adaptation while the vehicle is following pitch-only reference trajectories. In the second experiment, the pitch-only reference trajectory oscillates about zero pitch. In the third experiment, pitch-only reference trajectory oscillates about a pitch of 5° with an amplitude of 3°. Thus the second experiment requires thrust reversals to follow the specified reference trajectory, and the third experiment does not require thrust reversals. Figure 3 plots the angular velocity, thrust commands, and mass estimate derivative for both experiments. In the thrust subplots, the four lines are plotted. For the two thrusters actuating vehicle pitch, both the commanded and estimated thrusts are shown. Note that the thrust is estimated using a thruster's measured angular velocity as detailed in Section III-A. As seen in the left thrust plot, as the commanded thrust crosses zero, the measured output remains zero until the commanded thrust reaches 5 Newtons. The buoyancy torque's influence causes the pitch and y angular velocity to significantly deviate from their respective reference trajectories. From the perspective of the AMBC algorithm, these deviations from the position and velocity reference trajectories are indistinguishable from the deviations which would occur if the estimated pitch inertia were too large, thus the parameter estimate update for this term, $\dot{\hat{m}}_5$, have a large negative transient reponse after each thrust reversal. Over a multi-hour experiment this systematic error causes pitch and roll mass estimates to adapt to physically unrealistic negative values. In the four plots to the right in Figure 3 show that, without thrust reversals, the chain of events leading to a large negative transient response in the pitch mass update law are not present. The balanced parameter adaptation seen in this third experiment leads to pitch mass convergence to a physically realistic value.

D. Experimental Evaluation of Two-Step Method

In this subsection we report an experimental evaluation of the adaptive tracking control algorithm II-C. The first step is identifying the gravitational and buoyancy parameters for the UV using the adaptive tracking controller for plant model (12). The reference trajectory was constant in translational position and heading, with slow changes in pitch and roll to provide quasi-static motion. For this experiment we used a sinusoidal pitch reference trajectory with a magnitude of 0.2 rad and frequency of 34 Hz and a sinusoidal roll reference trajectory with a magnitude of 0.15 rad and frequency of 42 Hz. The gains used were $k_p = 300$, $k_d = 100$ $\gamma_g = \gamma_{b_1} = \gamma_{b_2} = 0.5$ and $\gamma_{b_3} = 10.0$. Over a 90 minute experiment the gravitational and buoyancy parameters converged to the values shown in Table IV.

TABLE IV: Gravitational Parameters Identified During Quasi-Static Motion

	g	b_1	b_2	b_3
Final	3.59 N	1.696 $N\,m$	3.09 $N\,m$	300 $N\,m$

Using the identified parameters from Table IV, we experimentally evaluated the performance of the two-step AMBC described in II-C. The reference trajectory specified was RefTraj1 from Table I. The mass and drag parameters were initialized to zero. The gains used were $k_p = 300$, $k_d = 1000$, $\gamma_{m_i} = 1000$ and $\gamma_{d_i} = 5000$. Over a four and a half hour experiment all 12 mass and drag parameters were observed to converge to physically realistic values. Table V records the initial and final value for each dynamic parameter.

Two-Step AMBC Trajectory Tracking Performance: Figure

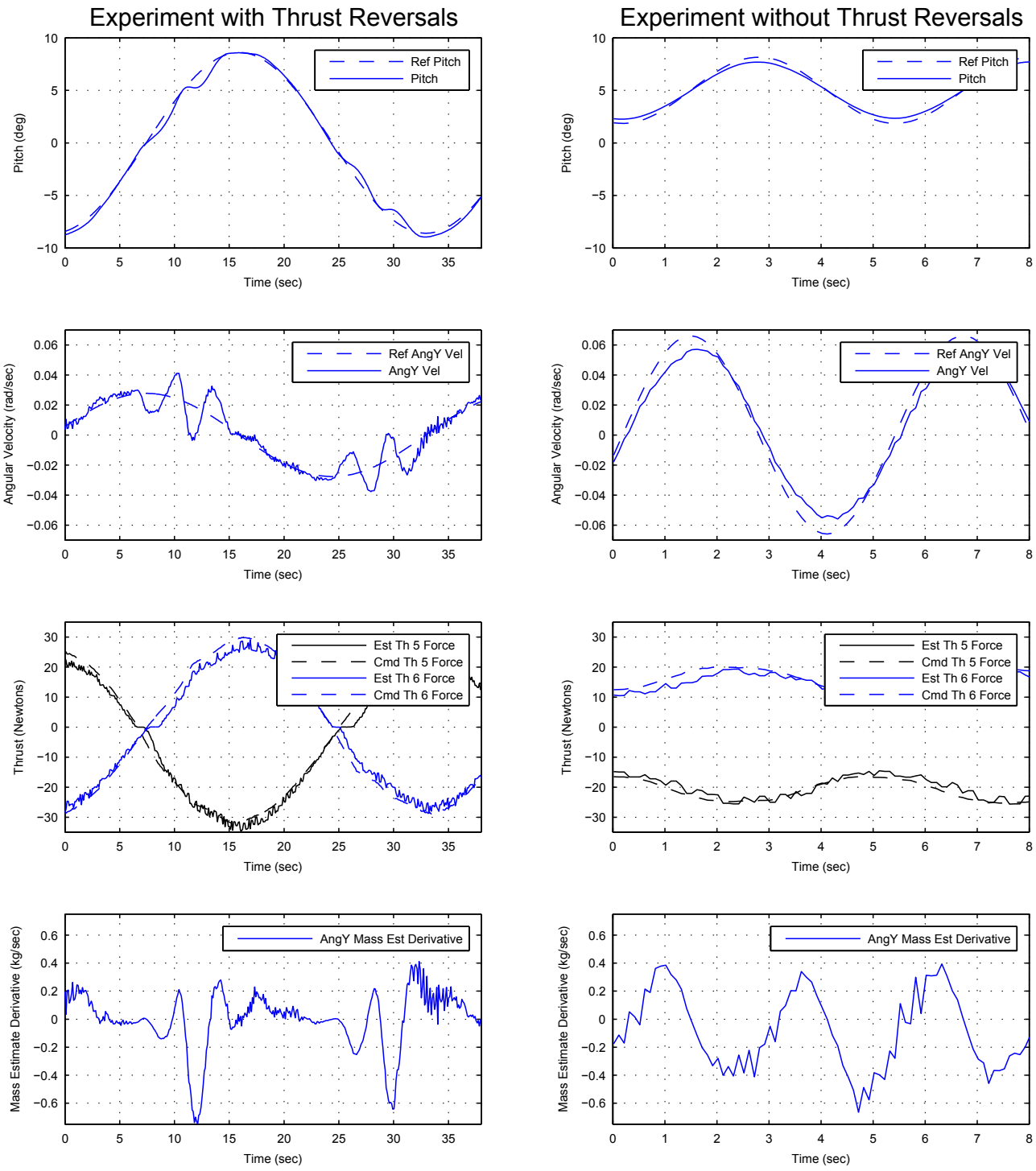

Fig. 3: Data from two experiments where AMBC was used to follow a single DOF reference trajectory in pitch. For both experiments an uncoupled model was assumed, initial parameter estimates taken from the final values in Tables IV and V, and thruster force was estimated using measured propeller angular velocity. The four plots on the left are from the same 40 second subset of a single experiment which had thrust reversals. In the left plot of commanded/estimated thruster output, a short period of thruster stiction is seen at each thrust reversal. The effects of thruster stiction are seen in both the pitch and angular velocity plots as deviations from each state's respective reference trajectory. In the left pitch mass update law plot, the parameter update law is seen to have a large negative transient response after each thurst reversal. The four plots on the right are from the same 8 second subset of a single experiment which did not have thrust reversals. The chain of events leading to a large negative transient response in the pitch mass update law are not present in this experiment.

TABLE V: Parameters Identified with two-step AMBC during Dynamic Motion Trajectory-Tracking

DOF	$m_i(t_o)$	$m_i(t_f)$	$d_i(t_o)$	$d_i(t_f)$
Tran X	0.0 kg	628 kg	0.0 $\frac{N\,s^2}{m^2}$	-1259 $\frac{N\,s^2}{m^2}$
Tran Y	0.0 kg	791 kg	0.0 $\frac{N\,s^2}{m^2}$	-1429 $\frac{N\,s^2}{m^2}$
Tran Z	0.0 kg	1043 kg	0.0 $\frac{N\,s^2}{m^2}$	-3083 $\frac{N\,s^2}{m^2}$
Ang X	0.0 $kg\,m^2$	95.7 $kg\,m^2$	0.0 $N\,s^2$	-727.1 $N\,s^2$
Ang Y	0.0 $kg\,m^2$	145.3 $kg\,m^2$	0.0 $N\,s^2$	-783.4 $N\,s^2$
Ang Z	0.0 $kg\,m^2$	110.2 $kg\,m^2$	0.0 $N\,s^2$	-465.6 $N\,s^2$

4 compares the performance of the two-step AMBC to a PDC with comparable gains. These two plots contain the exponential position and velocity MNE for the PDC and two-step AMBC experimental run. Both controllers were following the reference trajectory RefTraj1 from Table I as well as using $k_p = 300$ and $k_d = 100$ gains. The PDC MNE were calculated using 10 minutes of data. The MNE values for the two-step AMBC were calculated for consecutive 15 minutes windows. Due to page limit constraints, the trajectory tracking performance for each of the 12 individual DOF are not reported here but are available online [16].

Note that several hours were required for the the dynamic plant parameter estimates to converge to physically realistic values. Figure 4 presents the changes in trajectory-tracking performance during parameter adaptation. Since PDC trajectory-tracking performance does not adapt to the system as part of the control process, we see from the right side of Figure 4 that the asymptotic performance of two-step AMBC provides 30% better position tracking and 8% worse velocity tracking than PDC with similar gains.

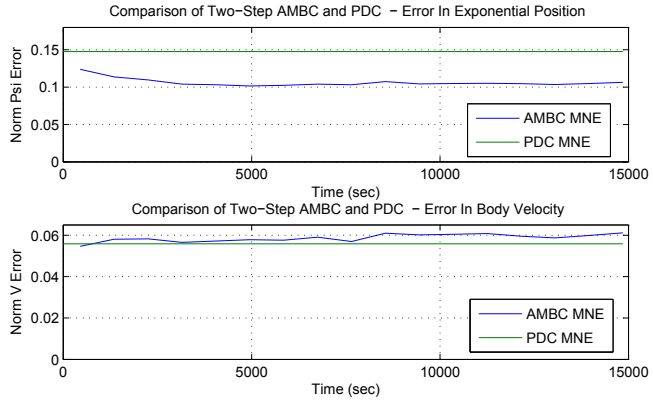

Fig. 4: Exponential position and velocity MNE data for two experimental controller evaluations, a PDC and the two-step AMBC. Both controllers were following the same reference trajectory (RefTraj1 from Table I) as well as using the gains $k_p = 300$ and $k_d = 100$. The PDC NME were calculated using 10 minutes of data, , this single value is plotted in green across the entire figure. The two-step AMBC MNE values were calculated for consecutive 15 minute windows and plotted in blue.

Two-Step AMBC Parameter Cross-Validation: In addition to providing trajectory tracking, AMBC has also been proposed to identify UV models. Figure 5 shows the ability of the identified model to match vehicle performance in forward simulation increases during parameter adaptation. Figure 5 shows experimentally measured states verses the states from numerical simulations; each numerical simulation uses a model identified by the two-step AMBC after a set amount of time. For this comparison, a PDC was used to drive the JHU ROV to follow RefTraj2 from Table I, the UV states and thrust inputs were recorded for 10 minutes. Each JHU ROV simulation used the thrust inputs recorded and initial JHU ROV states to create a forward simulation. Three states representative of the eight open-loop-stable states are plotted. Note that both in the plots and listed MAE values, the capacity of the identified parameters to model vehicle performance increases as time progresses. Although the models identified using two-step AMBC were not able to reproduce the highest frequency fluctuation's observed experimentally (such as those seen in the z angular velocity subplots of Figure 5), the states shown from simulating a model using the "5000 sec" parameter set (the final parameter set included in this analysis) indicate that AMBC can produce parameter estimates which result in accurate plant models.

IV. CONCLUSION

In this paper we report an experimental investigation of a previously unreported UV AMBC failure mode where unmodeled thruster dynamics during thrust reversals cause unstable parameter adaptation. We also report a novel two-step AMBC algorithm which is shown experimentally to provide stable trajectory tracking and parameter adaptation in the presence of the unmodeled thruster dynamics of our system. Finally, we report a comparative experimental analysis of the two-step AMBC algorithm with PDC. This experimental evaluation shows that two-step AMBC provides 30% better position tracking performance and 8% worse velocity tracking performance over PDC.

REFERENCES

[1] G. Antonelli, S. Chiaverini, N. Sarkar, and M. West, "Adaptive control of an autonomous underwater vehicle: Experimental results on ODIN," *IEEE Transactions on Control Systems Technology*, vol. 9, no. 5, pp. 756–65, September 2001.

[2] R. Bachmayer, L. L. Whitcomb, and M. Grosenbaugh, "An accurate finite-dimensional dynamical model for the unsteady dynamics of marine thrusters," *IEEE Journal of Oceanic Engineering*, vol. 25, no. 1, pp. 146–159, January 2000.

[3] F. Bullo and R. M. Murray, "Proportional derivative (PD) control on the Euclidean group," California Institute of Technology, Tech. Rep., 08 1995.

[4] N. Chaturvedi, D. Bernstein, J. Ahmed, F. Bacconi, and N. McClamroch, "Globally convergent adaptive tracking of angular velocity and inertia identification for a 3-DOF rigid body," *IEEE Transactions on Control Systems Technology*, vol. 14, no. 5, pp. 841 –853, Sept. 2006.

[5] J. J. Craig, P. Hsu, and S. Sastry, "Adaptive control of mechanical manipulators," *The International Journal of Robotics Research*, vol. 6, no. 2, pp. 16–28, Summer 1987.

[6] T. I. Fossen and S. I. Sagatun, "Adaptive control of nonlinear underwater robotic systems," in *Proceedings of the IEEE International Conference on Robotics and Automation*, apr 1991, pp. 1687 –1694 vol.2.

[7] T. I. Fossen, *Guidance and Control of Ocean Vehicles*. New York: John Wiley and Sons, 1994.

[8] A. J. Healey, S. M. Rock, S. Cody, D. Miles, and J. P. Brown, "Toward an improved understanding of thruster dyamics for underwater vehicles," *IEEE Journal of Oceanic Engineering*, vol. 20, no. 4, pp. 354–61, October 1995.

[9] IXSEA, *PHINS III User Guide*, 5th ed., IXSEA, July 2008.

[10] J. Kim and W. K. Chung, "Accurate and practical thruster modeling for underwater vehicles," *Ocean Engineering*, vol. 33, no. 5, pp. 566–586, 2006.

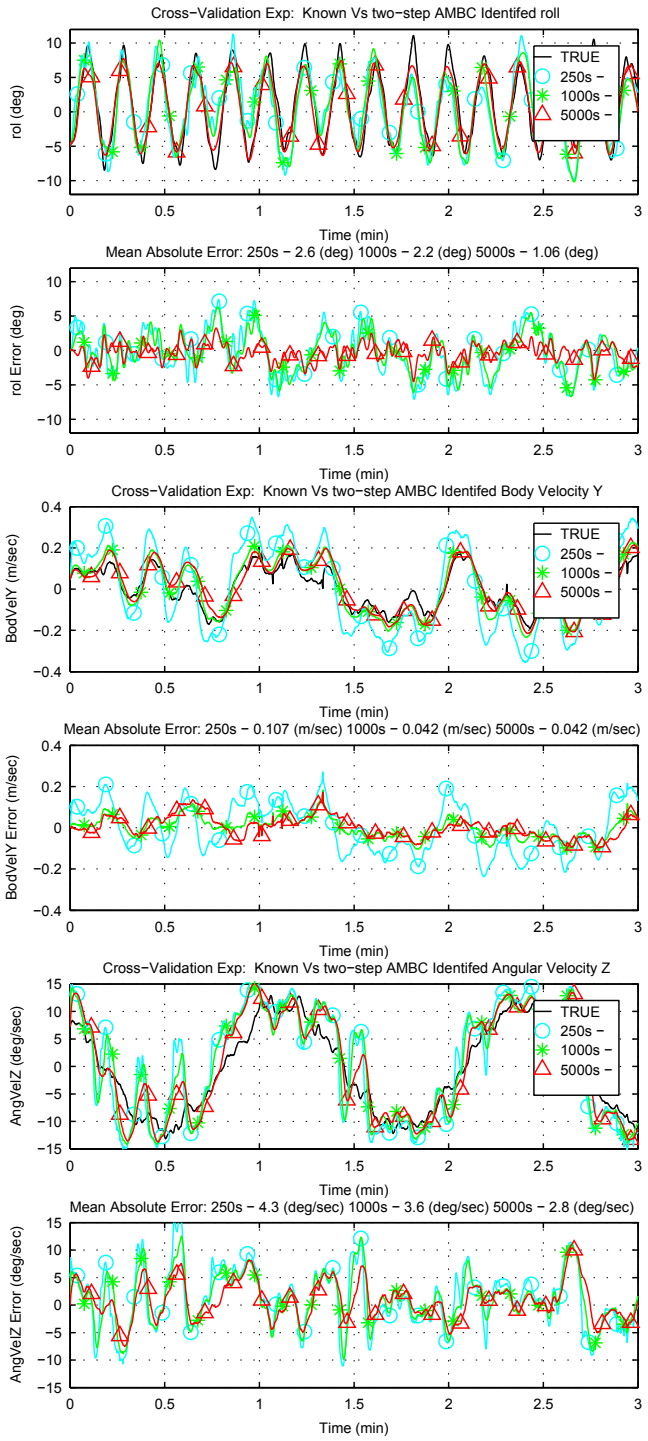

Fig. 5: Representative data of experimental and simulated JHU ROV states during 6 DOF dynamic operation. In the roll, y body velocity and z angular velocity plots, the measured state is plotted together with the position estimates from three JHU ROV simulations. The three parameter sets were taken from the time history of parameter adaptation recorded during the two-step AMBC experiment. The '250s' parameter set (plotted in blue and marked with circles) is the forward simulation using parameters identified after 250 seconds of parameter adaptation. Similarly the '1000s' (plotted in green and marked with stars) and '5000s' (plotted in red and marked with triangles) are the forward simulations using parameters identified after 1000 and 5000 seconds of parameter adaptation respectively. For each DOF, the error between the measured positions and their estimates is shown.

[11] J. C. Kinsey, D. A. Smallwood, and L. L. Whitcomb, "A new hydrodynamics test facility for UUV dynamics and control research," in *Proceedings of IEEE/MTS Oceans*, San Diego, CA, September 2003, pp. 356–361.

[12] D. E. Koditschek, "Adaptive strategies for the control of natural motion," in *IEEE Proceedings 24th Conference on Decision and Control*, Fort Lauderdale, Dec 1985, pp. 1405–1409.

[13] D. Maalouf, I. Tamanaja, E. Campos, A. Chemori, V. Creuze, J. Torres, L. Rogelio, *et al.*, "From PD to nonlinear adaptive depth-control of a tethered autonomous underwater vehicle," in *IFAC Joint conference 2013*, 2013.

[14] S. C. Martin and L. L. Whitcomb, "Experimental identification of six-degree-of-freedom coupled dynamic plant models for underwater robot vehicles," *IEEE Journal of Oceanic Engineering*, vol. PP, no. 99, pp. 1–10, 2013.

[15] ——, "Preliminary experiments in fully actuated model based control with six degree-of-freedom coupled dynamical plant models for underwater vehicles," in *Proceedings of the IEEE International Conference on Robotics and Automation*, Karlsruhe, Germany, May 2013.

[16] C. J. McFarland, "Adaptive identification and control for underwater vehicles: Theory and experimental evaluations," Ph.D. dissertation, The Johns Hopkins University, Baltimore, MD USA, November 2013.

[17] R. M. Murray, Z. Li, and S. S. Sastry, *A Mathematical Introduction to Robotic Manipulation*. Boca Raton: CRC Press, 1994.

[18] K. Narendra and A. Annaswamy, *Stable Adaptive Systems*. NY: Prentice-Hall, 1988.

[19] G. Niemeyer and J.-J. E. Slotine, "Performance in adaptive manipulator control," *The International Journal of Robotics Research*, vol. 10, no. 2, pp. 149–161, April 1991.

[20] RD-Instruments, "Workhorse Navigator Datasheet," Teledyne RD-Instruments, http://www.rdinstruments.com/navigator.aspx.

[21] C. Rohrs, L. Valavani, M. Athans, and G. Stein, "Robustness of continuous-time adaptive control algorithms in the presence of unmodeled dynamics," *IEEE Transactions on Automatic Control*, vol. 30, no. 9, pp. 881–889, 1985.

[22] N. Sadegh and R. Horowitz, "Stability and robustness analysis of a class of adaptive controllers for robotic manipulators," *The International Journal of Robotics Research*, vol. 9, no. 3, pp. 74–92, June 1990.

[23] J.-J. E. Slotine and M. D. Di Benedetto, "Hamiltonian adaptive control of spacecraft," *IEEE Transactions on Automatic Control*, vol. 35, no. 7, pp. 848 –852, jul 1990.

[24] J.-J. E. Slotine and W. Li, "On the adaptive control of robot manipulators," *The International Journal of Robotics Research*, vol. 6, no. 3, pp. 49–59, Fall 1987.

[25] D. A. Smallwood and L. L. Whitcomb, "Model-based dynamic positioning of underwater robotic vehicles: theory and experiment," *IEEE Journal of Oceanic Engineering*, vol. 29, no. 1, pp. 169–186, 2004.

[26] J. D. Van Manen and P. Van Ossanen, *Principles of Naval Architecture, Second Revision, Volume II: Resistance, Propulsion, and Vibration*. Jersey City, New Jersey USA: Society of Naval Architects and Marine Engineers, 1988, E. V. Lewis, Editor.

[27] L. L. Whitcomb, A. Rizzi, and D. E. Koditschek, "Comparative experiments with a new adaptive controller for robot arms," *IEEE Transactions on Robotics and Automation*, vol. 9, no. 1, pp. 59–70, February 1993.

[28] D. R. Yoerger, J. G. Cooke, and J. E. Slotine, "The influence of thruster dynamics on underwater vehicle behavior and their incorporation into control system design," *IEEE Journal of Oceanic Engineering*, vol. 15, no. 3, pp. 167–178, June 1990.

[29] D. R. Yoerger and J. E. Slotine, "Adaptive sliding control of an experimental underwater vehicle," in *Proceedings of the IEEE International Conference on Robotics and Automation*, Sacremento, CA, USA, April 1991, pp. 2746–2751.

[30] D. R. Yoerger and J.-J. E. Slotine, "Robust trajectory control of underwater vehicles," *IEEE Journal of Oceanic Engineering*, vol. OE-10, no. 4, pp. 462–70, October 1985.

[31] J. Yuh, "Modeling and control of underwater robotic vehicles," *IEEE Transactions on Systems, Man, and Cybernetics*, vol. 20, no. 6, pp. 1475 –1483, nov/dec 1990.

[32] J. Yuh, J. Nie, and C. S. G. Lee, "Experimental study on adaptive control of underwater robots," in *Proceedings of the IEEE International Conference on Robotics and Automation*, vol. 1, 1999, pp. 393–398 vol.1.

[33] S. Zhao and J. Yuh, "Experimental study on advanced underwater robot control," *IEEE Transactions on Robotics*, vol. 21, no. 4, pp. 695–703, 2005.